

# THE EFFECT OF WALL THERMAL BOUNDARY CONDITION ON NATURAL CONVECTIVE SHUTDOWN COOLING IN A GAS TURBINE

**Daniel D. Fahy\***

Oxford Thermofluids Institute  
Department of Engineering Science  
University of Oxford  
Oxford, UK  
Email: daniel.fahy@eng.ox.ac.uk

**Prof. Peter Ireland**

Oxford Thermofluids Institute  
Department of Engineering Science  
University of Oxford  
Oxford, UK

## ABSTRACT

*As a civil gas turbine cools down, asymmetric natural convective heat transfer causes the bottom sector of the rotor to cool faster than the top; this circumferential thermal gradient can potentially cause the shaft to deflect – a phenomenon called thermal or rotor bow. Rotor bow is tremendously difficult to predict due to its dependence on a number of engine design parameters, in addition to the complex nature of natural convective flows.*

*A novel experimental facility has been developed to gain further understanding into shutdown cooling of a gas turbine. The scope of this paper is to quantify the effect of basic design features on natural convective cooling in an engine annulus during shut-down; specifically the influence of the thermal boundary wall conditions and the annular diameter ratio. In addition to this, a low-cost, robust thermocouple probe has been developed and validated, which allows for accurate temperature measurements in a natural convective boundary layer.*

*An extensive experimental campaign has been completed. The key finding is that the local radial wall temperature difference was found to be the most influential parameter on the local heat transfer. Non-isothermal walls did not alter the overall distribution of the inner wall equivalent conductivity. This was true for both cylindrical and conical sections. An appropriate characteristic length for use in the Rayleigh number definition for both the concentric cylinder and conical sections have been validated. The conical inner section ( $5^\circ$  hade angle) did not affect the overall heat transfer in the range of conditions tested. Therefore, the mean surface heat transfer for non-isothermal inner and outer profiles, within the range  $-0.4 < \Delta Ra / Ra_{L_c} < 0.4$ , where the thermal gradient is negative in the clockwise from top-dead-centre, can be predicted using isothermal correlations for  $Ra_{L_c} < 5.0 \times 10^5$  and  $Dr \leq 1.5$ .*

## NOMENCLATURE

$A$	Linear fit coefficient (K)
$B$	radial temperature gradient: $dT/dr$ (K/m)
BDC	Bottom-dead-centre: $\theta = 180^\circ$
$D$	Diameter (m)
$Dr$	Diameter ratio. $D_o/D_i$
$g$	Acc. due to gravity ( $m/s^2$ )
$k$	Thermal conductivity (W/mK)
$k_{eq}$	Equivalent conductivity $\dot{q}_{conv}/\dot{q}_{cond}$
$\bar{k}_{eq}$	Mean surface equivalent conductivity
$L_c$	Characteristic length (m)
$L_n$	Probe wire length (m)
$N$	Number of data points used in curve fitting
$Nu$	Nusselt number
$\dot{q}$	Heat flux ( $W/m^2$ )
$Q$	Heat power per unit of axial length (W/m)
$r$	Radius (m)
$Ra$	Rayleigh number $g\beta(T_{i,\theta} - T_{m,\theta})L_c^3/\nu\alpha$
$\bar{Ra}$	Mean surface Rayleigh number
$\Delta Ra$	Rayleigh number difference from top to bottom
$T$	Temperature (K)
$T^*$	Non-dimensional temperature
$\Delta T_c$	Temperature difference from top to bottom (K)
$\Delta T_r$	Local radial temperature difference (K)
TDC	Top-dead-centre: $\theta = 0^\circ$
$x$	Radial distance m
$\alpha$	Thermal diffusivity ( $m^2/s$ )
$\beta$	Volumetric expansion coefficient ( $1/K$ )
$\nu$	Kinematic viscosity ( $m^2/s$ )
$\sigma$	Uncertainty
$\theta$	Surface angle ( $^\circ$ )

\*Address all correspondence to this author.

## Subscripts

$b$	$\theta = 180^\circ$
$cond$	Conduction
$conv$	Convection
$i$	Inner cylinder
$o$	Outer cylinder
$m$	Mid-annulus
$sp$	Temperature setpoint
$t$	$\theta = 0^\circ$
$w$	Wire

## INTRODUCTION

As a large civil gas turbine is cooling following operation, natural convection causes the lower section of the rotor to cool faster than the upper section. Over a period of time, typically 30 minutes to 3 hours after shutdown, differential axial thermal expansion between top-dead-centre (TDC) and bottom-dead-centre (BDC) causes the shaft to deflect. This phenomenon is known as rotor or thermal bow. Attempts to restart an engine whilst it is in this bowed state can lead to a number of issues related to vibrational rotor dynamics and even tip rubs in severe cases. All engines are affected by rotor bow to some degree, however the severity, duration and onset-time of this effect is usually unknown until full scale engine testing begins—potentially delaying engine development. The scope of this paper is to quantify the effect of basic design features on natural convective cooling in an engine annulus during shutdown. The compressor annulus geometry is an obvious starting point for exploration as it is usually in this location that the consequences of rotor bow are detected. It is well approximated by concentric cylinders and conical sections.

A recent extensive parametric computational study focusing on helicopter engines, conducted by Smith *et al.* [1], determined that the rotor diameter and length were the parameters that had the greatest impact on rotor bow onset and severity. This work also highlighted the complex nature of the flow and interdependency of a large number of design features. Pilkington [2] has recently developed a turbulent heat flux model that improves the numerical prediction of natural convection in a gas turbine.

The literature is rich with both numerical and experimental natural convection studies of concentric and isolated cylinders. Predicting natural convective flows has proven to be very difficult owing to the non-linear nature of the problem, strong coupling of momentum and energy equations, and sensitivity to boundary conditions [3]. The majority of experimental studies are on small scale, isothermal test pieces. This paper will investigate the influence of the thermal boundary wall conditions, and also the diameter ratio of the cylinders ( $Dr = D_o/D_i$ ). Powe *et al.* [4] concluded that there are three distinct flow structures regions for natural convection in a horizontal concentric annulus, based on the diameter ratio. Two of those regions are applicable to large gas turbine compressor geometry. The boundary between flow structure regions is at  $Dr = 1.24$ . Natural convection from a cone has been rarely studied. Oosthuizen [5] hypothesised that at low hade angles, the heat transfer from a cone may be approximated as a summation of 2D cylindrical sections. However, this is yet to be validated.

## EXPERIMENTAL FACILITY

An experimental facility has been built which can simulate the natural convective flow field in a section of the main gas path of a civil gas turbine compressor during shutdown. Figures 1 and 2 provide outlines of the experimental facility. The inner assembly has a cylindrical section, and a  $5^\circ$  conical section. Three unique outer cylinders can be installed to allow for testing at different diameter ratios. The inner cylinder diameter is 326 mm; the overall axial length of the annulus is 640 mm. This geometry is a good approximation to a typical civil gas turbine high-pressure compressor.  $\theta$  is defined as  $0^\circ$  at TDC, and positive clockwise.

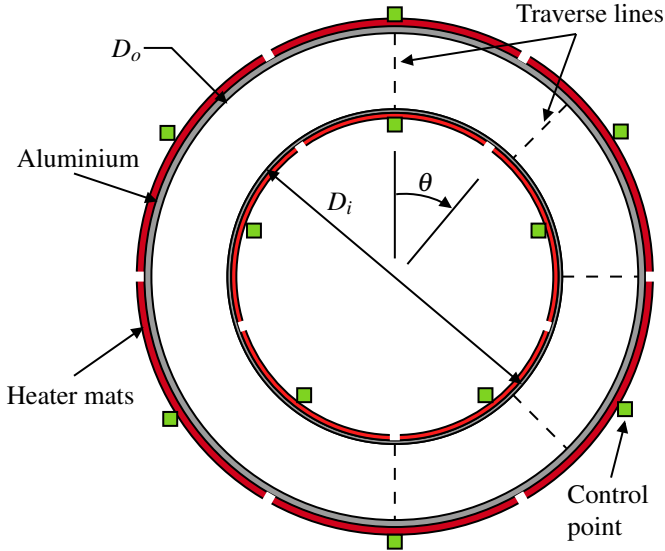
Heater mats are used to control the inner and outer wall thermal boundary conditions. The inner surface has five mats circumferentially; the outer wall has six. The power to each individual mat is modulated using a PID control loop system that uses a type K thermocouple embedded into the metal (using high conductivity epoxy) as the feedback signal. This system allows for uniform and circumferentially-varying temperature distributions on both walls to be defined. This design is advantageous as it decouples the convective heat transfer from the conductive heat transfer that occurs in a gas turbine during shutdown. It allows for the evaluation of the circumferential distribution of convective heat flux for a given surface temperature profile and diameter ratio; thus the findings are applicable as a boundary condition for a conduction calculation of the internal rotor drum geometry of any engine.

The inner cylinder and cone sections are mounted through six point contacts to minimise end conduction. Guard heaters were also embedded into the contact points but were found to have a negligible effect. The maximum control point temperature is 370 K. Top-to-bottom gradients of up to 20 K can be defined. The circumferential temperature distribution is modelled as a cosine profile by specifying values at each control point. The gradient of temperature is always negative as  $\theta$  increases, as this is most representative of a shutdown cooling cycle.

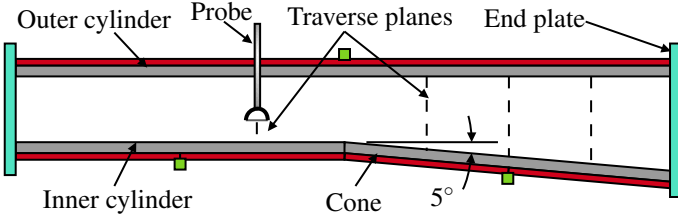
A five-axis radial traverse system is used to measure the air temperature profiles at  $45^\circ$  intervals. The system can be moved to different axial planes, as indicated by the dashed lines shown in figure 2. The probe head location repeatability has been tested and found to be  $< 0.1$  mm. The five radial traverses are completed simultaneously using a timing belt system. Traverses with an individual probe can also be completed. A comparison of both methods is discussed further in the results section.

Figure 3 shows the installed facility. The ends of the annulus are sealed using acrylic end plates and steel tie rods. The shaft-mounted design allows the inner assembly to be rotated. Tests repeated at different inner rotations have shown that the results are independent of the inner assembly orientation. A thin layer of rohacell, which is a very low conductivity structural foam ( $0.03 \text{ W/m}^2\text{K}$ ), is adhered to the inner cylinder outer surface. This is used for infrared experiments [6].

During a shutdown cycle, an engine will experience a range of Rayleigh numbers. This experimental facility can operate with Rayleigh numbers in the range:  $Ra_{Lc} = 7.5 \times 10^3 - 1.2 \times 10^6$ ; While the diameter of the experimental facility is roughly half the size of a typical large civil compressor, crucially, the diameter ratios ( $Dr$ ) are matched as this parameter has a strong influence



**FIGURE 1.** Cross-sectional schematic of the experimental facility.  $\theta$  is positive clockwise from top-dead-centre.



**FIGURE 2.** Annular cross-section of the upper area experimental rig. The dashed lines represent the traverse planes.

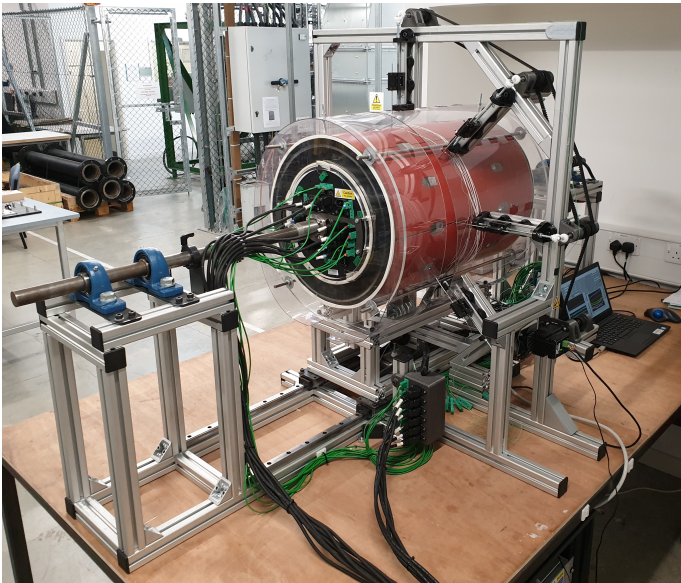


**FIGURE 3.** Installation of the experimental facility.

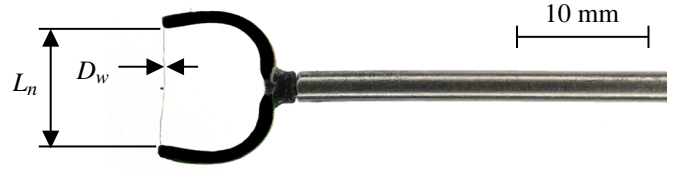


**FIGURE 4.** Boundary layer thermocouple probe.

on the overall flow structure. This in turn means that the characteristic length,  $L_c$ , defined in equation 10 is matched. Therefore,  $Ra_{L_c}$  is only slightly below the peak value of an engine, due to the lower temperatures of the experiment.

### Instrumentation

George and Capp [7] developed a theory for natural convective boundary layers. The section of the thermal boundary layer that is closest to the wall (coined the conductive sub-layer) is linear in the direction normal to the wall. Heat transferred by conduction dominates in this layer and consequently, the slope of thermal boundary layer in this region is proportional to the local heat flux (Fourier's law):

$$\dot{q} = -k \frac{dT}{dr} \quad (1)$$

Therefore, a thermocouple traverse normal to the wall boundary layer can be used to determine the local heat flux. This theory has been validated experimentally. A low-cost, robust thermocouple probe has been developed which will allow for accurate temperature measurements in a natural convective boundary layer. Kulkarni *et al.* [8] have designed a similar probe for forced convective boundary layer probes. Their numerical work concludes that conduction away from the hot junction is the dominant source of error. They also show that the flow field distortion due to the close proximity of the heated wall is not significant [9]. Conduction away from the hot junction is caused by strong thermal gradient near the wall. This error can be reduced by designing the probe mount to have a length of wire ( $L_n$ ) parallel to the wall. Figure 4 shows a schematic of the probe. The black mounting heads are manufactured on a resin 3D printer. A 76  $\mu\text{m}$  type K thermocouple is used due to its small conducting cross-sectional area, low cost and robustness.

The optimum value of  $L_n$  has been determined using a combination of a detailed 1D heat conduction model of the thermocouple and experiments. Figure 5 shows an experimental temperature traverse for three different values of  $L_n$ . Non-dimensional temperature is defined by equation 2.  $T^*$  is not equal to 1 at the wall due to the temperature drop across the layer of rohacell.

$$T^* = \frac{T - T_{o,\theta}}{T_{i,\theta} - T_{o,\theta}} \quad (2)$$

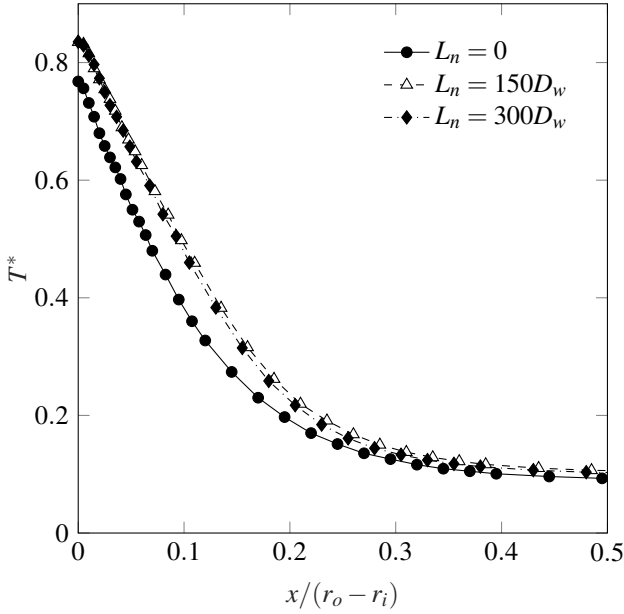


**FIGURE 5.** Experimental radial temperature profile at  $\theta = 180^\circ$  and for the three different values of  $L_n$ .  $Ra_{L_c} = 1.5 \times 10^5$  and  $Dr = 1.25$ .

An increase in  $L_n$  by  $150D_w$  from standard thermocouple design ( $L_n = 0$ ) has increased the temperature readings significantly in the region where there is a strong fluid temperature gradient; in the mainstream flow, where this gradient no longer exists, both probe give similar results. This finding confirms the the conduction is indeed a strong source of error in the thermal boundary layer measurements. Increasing  $L_n$  further to  $300D_w$  did not yielded the same profile as the  $150D_w$  probe. Therefore, a probe with an  $L_n$  of  $150D_w$  was used in this experimental campaign. Data was recorded for 40 seconds at 4 Hz at a given traverse point. This was deemed adequate as the standard deviation of the measurement converged to an adequate value.

During shutdown cooling, radiative heat transfer should not be neglected when attempting to evaluate the severity of the rotor bow for a particular engine. However, the radiation characteristics of each engine will be different. This traverse technique is advantageous as it measures the convective heat flux to the air directly; thus, the findings are in turn decoupled from the radiative heat transfer in the experiment. This is beneficial for the same reasoning as to why the rotor internal conduction is not modelled, as both radiation and conduction can be included in a thermal model of a specific engine. It is also worth noting here that it is the asymmetry of the natural convective cooling that causes rotor bow, while both conduction and radiation tend to be axisymmetric.

## Uncertainty

A least squares fitting method is used to fit a line ( $T = A + Bx$ ) to the conductive sub-layer and thus determines the linear gradient of temperature ( $dT/dr$ ). The slope is of the line is calculated as:

$$B = \frac{N \sum xT - \sum x \sum T}{\sum x^2 - (\sum x)^2} \quad (3)$$

where  $B = dT/dr$  and  $N$  is the number of points used to fit the curve. It is assumed that the uncertainty in measurements of  $T$  are equal, which is justifiable since it is the same thermocouple. Least squares fitting usually assumes that the uncertainties in the  $x$  measurements are negligible. The uncertainty in  $x$  can then be accounted for by converting it to an equivalent uncertainty in terms of temperature:  $B\sigma_x$  [10]. This assumes that all uncertainties in  $x$  are equivalent, again a reasonable assumption. The uncertainty of the probe position ( $x$ ) is 0.1 mm. The uncertainty of the measured temperature  $T$  is given by equation 4.

$$\sigma_T = \left[ \frac{1}{N-2} \sum_{n=1}^N (T_n - A - Bx_i)^2 + (B\sigma_x)^2 \right]^{1/2} \quad (4)$$

The bias error of the thermocouple probe can also be examined. A type K thermocouple calculates temperature by fitting a linear curve to a measured voltage signal:  $T = V_o + GV$ . The quoted accuracy of this type of thermocouple ( $2\sigma_{TC}$ ) is  $\pm 2^\circ\text{C}$  or  $\pm 0.75\%$ , over a temperature range of  $-270$  to  $1260^\circ\text{C}$ . Any uncertainty in  $V_o$  will have no effect on the calculation of  $\dot{q}$  as it depends on a temperature gradient. If it assumed that all of the inaccuracy is in the gain ( $G$ ), then the maximum error of the true temperature slope is  $\pm 0.6\%$ . This highlights the advantage of this measurement technique. Using the method of propagation of errors applied to the equation 3, the uncertainty in  $dT/dr$  is:

$$\sigma_B = \sqrt{\frac{N}{\sum x^2 - (\sum x)^2} \sigma_T^2} \quad (5)$$

This gave an uncertainty range of 3.5 to 14% to a 95% confidence interval ( $\pm 2\sigma_B$ ). A higher uncertainty was present in the top section of the annulus, due to the increased unsteadiness of the flow.

## Analysis

There is some variation in the literature in the choice of the most appropriate characteristic length and temperature difference in the Rayleigh number definition for a cylindrical annulus. Amongst others, the inner diameter, gap height and hydraulic diameter have all been used. The selection is complicated further in this study due to the inclusion of non-isothermal boundary conditions as well as a conical section. Equivalent conductivity is an intuitive way to interpret the natural convective heat transfer in an annulus. It is defined as the ratio of the convective heat transfer to the heat transfer that would occur by conduction only [11]. The solution of steady-state heat conduction in a 2D cylindrical annulus is:

$$Q_{cond} = \frac{2\pi k (T_1 - T_2)}{\ln(r_2/r_1)} \quad (6)$$

Converting this to a local heat flux and combining it with equation 1 gives the following expression for local equivalent conductivity at a surface:

$$k_{eq,\theta} = \frac{\dot{q}_{conv}}{\dot{q}_{cond}} = \frac{r(dT/dr) \ln(r_2/r_1)}{T_{1,\theta} - T_{2,\theta}} \quad (7)$$

For this experimental campaign, the inner surface values are used for the subscript 1. The mean of the local radial wall temperature difference is used as  $T_2$ , i.e.  $(T_{i,\theta} + T_{o,\theta})/2$ . Consequently, the mean radius is used as  $r_2$ . Non-dimensionalising the heat transfer by equation 7 is advantageous as it is intuitive, and  $dT/dr$  is measured directly from this experimental setup. Moreover, it can also be applied to the conical section of the rig at a 2D plane. Equivalent conductivity can be converted to a Nusselt number using the following equation:

$$Nu = k_{eq} \frac{2}{\ln(r_2/r_1)} \quad (8)$$

From this equation, it can be inferred that the equivalent conductivity is identical to using  $r_1 \ln(r_2/r_1)$  as the length scale in the standard Nusselt number definition. It seems appropriate to use the local temperature gradient  $(T_{i,\theta} - T_{m,\theta})$  in the definition of the local Rayleigh number. Fluid properties are calculated at the area-weighted average of the inner and outer wall temperature profiles.

$$Ra_{L_c} = \frac{g\beta(T_{i,\theta} - T_{m,\theta})L_c^3}{\nu\alpha} \quad (9)$$

The characteristic length is calculated using equation 10, which was first proposed by Itoh *et al.* [12]. The heat transfer in a concentric annulus has been shown to depend on both the inner diameter and the gap width. For example, a larger gap width increases heat transfer for a given inner diameter. This length scale accounts for changes in both parameters. It also approaches the gap width as  $r_1$  approaches  $r_2$ , which is the correct trend. The application of this will be commented on later, once the results are presented. Table 1 shows geometric information for the different traverse planes.

$$L_c = \sqrt{r_i r_o} \ln(r_o/r_i) \quad (10)$$

**TABLE 1.** Diameter ratios and characteristic lengths for the different test conditions

Cylinder		Cone	
$L_c$ (mm)	$Dr$	$L_c$ (mm)	$Dr$
39.9	1.25	46.8	1.30
59.8	1.37	53.8	1.36
		73.5	1.50

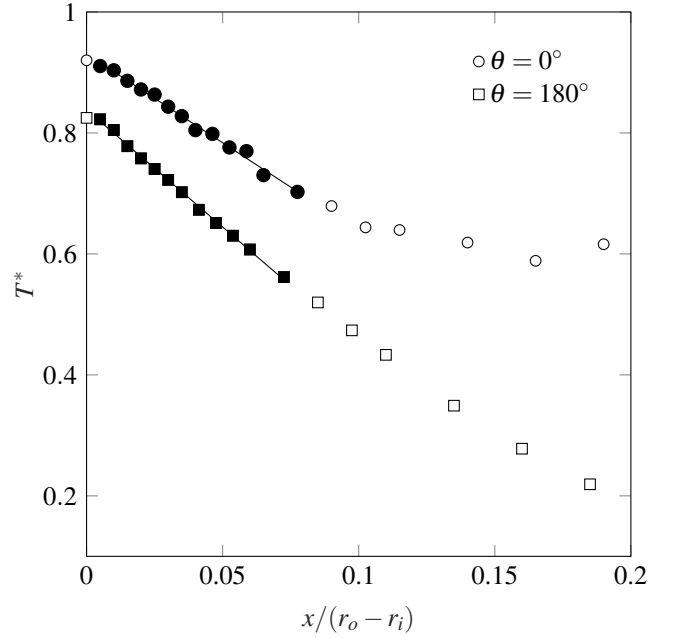


**FIGURE 6.** Radial temperature profiles for  $\theta = 0, 180^\circ$  traverse lines at  $Ra_{L_c} = 1.2 \times 10^5$  and  $Dr = 1.25$ , on the concentric cylinder plane. The filled markers indicate the points used in the line fitting.

## RESULTS

Figure 6 shows an example of a temperature traverse of the inner boundary layer at two values of  $\theta$  for  $Ra_{L_c} = 1.2 \times 10^5$ . The linear section of the conductive sub-layer is clearly visible. The filled markers indicate the points used to determine  $dT/dr$ . This is encouraging as it indicates the intrusion of the probe has not affected the flow regime.

The repeatability of the experimental facility can be quantified by examining figure 7. It shows a radial temperature profile at  $\theta = 45^\circ$  for  $Ra_{L_c} = 1.2 \times 10^5$  at  $Dr = 1.25$ . The experiments were completed of different days. This value of  $\theta$  was chosen as the largest unsteadiness in air temperatures was observed at this location. The five probes were traversed simultaneously for both runs 1 and 2; whereas the 'Individual' traverse had only the probe at  $45^\circ$  traversing. The test cases are near identical – especially in the conductive sub-layer. This confirms that acquiring the five radial temperature profiles simultaneously does not influence the measurements. In addition, the results are very repeatable.

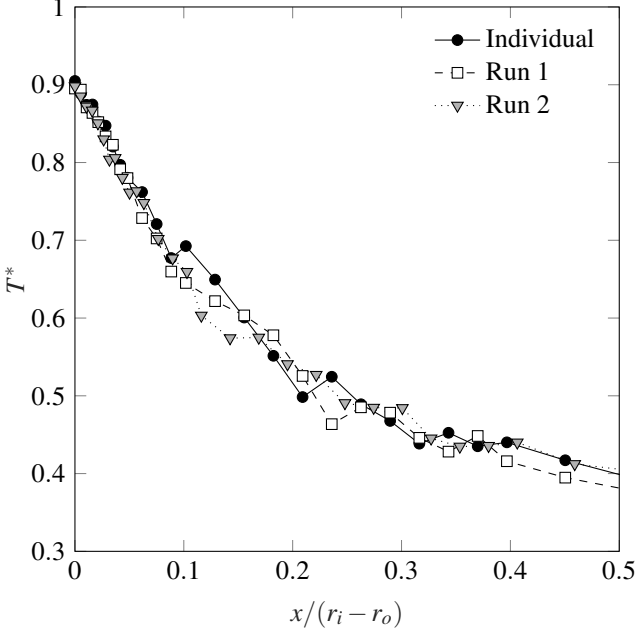


**FIGURE 7.** Radial temperature profiles at  $\theta = 45^\circ$  and  $Dr = 1.25$ . The five probes were traversed simultaneously for runs 1 and 2, whereas only the probe at  $45^\circ$  was traversed for the individual test.

### Non-Isothermal Boundary Conditions

As mentioned previously, the surface temperature distributions are defined using a cosine profile. The value at a given control point is given by:

$$T_{sp} = \left( T_{\theta=0} - \frac{\Delta T_c}{2} \right) + \frac{\Delta T_c}{2} (\cos \theta) \quad (11)$$

In all non-isothermal cases, the absolute value of the temperature decreased as  $\theta$  increases. Three values of  $\Delta T_c$  have been considered in this study: 0, 10, 20 K. Defining  $\Delta Ra$  as  $Ra_{L_c}(\theta = 0) - Ra_{L_c}(\theta = 180)$ , non-isothermal cases within the following range were conducted:  $-3.5 \times 10^4 < \Delta Ra < 7.2 \times 10^4$ . The initial series of tests, termed Tc, represent a full factorial design space for  $\Delta T_{c,i}$  and  $\Delta T_{c,o}$  at the three values mentioned above.  $Ra_{L_c}$  at  $\theta = 0^\circ$  is held constant in all nine cases:  $1.2 \times 10^5$ . The details of these tests are shown in table 2. All tests were completed at the concentric cylinder plane at  $Dr = 1.25$ . The findings from this campaign (see figure 8) can become somewhat obscured when the heat flux is non-dimensionalised as defined previously – as the local radial difference ( $\Delta T_r$ ) is different for the non-isothermal cases. Therefore, the heat flux as defined by equation 1 is used for clarity.

The inner wall heat flux in the lower section of the annulus varies significantly. However, the most striking finding from this campaign is that  $\dot{q}_i$  at TDC, where  $Ra_{L_c}$  is constant, remains relatively unchanged for all nine cases – the standard deviation of  $\dot{q}_{\theta=0}$  is  $< 8 \text{ W/m}^2$ . In case G, the heat flux at  $180^\circ$  is 85% higher than the value at  $0^\circ$ ; in contrast,  $\dot{q}$  at  $180^\circ$  is 35% lower than TDC in case C. It appears that the heat flux at  $0^\circ$  is invariable to either  $\Delta T_{c,i}$  or  $\Delta T_{c,o}$  over the range that was tested.

**TABLE 2.** Thermal boundary conditions for the Tc test cases shown in figure 8. All  $\Delta T$  numbers are in Kelvin.  $Ra_{L_c}$  at  $\theta = 0^\circ$  is held constant at  $1.2 \times 10^5$  in all nine cases.

	Key	$\Delta T_{c,i}$	$\Delta T_{c,o}$	$\Delta T_{r,t}$	$\Delta T_{r,b}$	$\Delta Ra$
A	●	0	0	40	40	0
B	■	10	0	40	30	$-3.2 \times 10^4$
C	▼	20	0	40	20	$-6.3 \times 10^4$
D	○	0	10	40	50	$3.2 \times 10^4$
E	□	10	10	40	40	0
F	▽	20	10	40	30	$-3.0 \times 10^4$
G	⊙	0	20	40	60	$6.2 \times 10^4$
H	⊠	10	20	40	50	$3.0 \times 10^4$
I	⊖	20	20	40	40	0

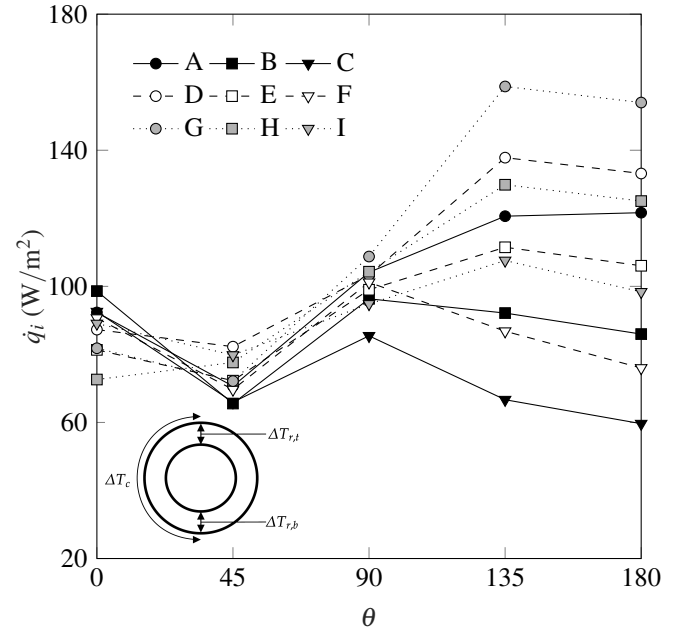


**FIGURE 8.** Inner wall convective heat flux for various thermal boundary condition tests where  $Ra_{L_c}$  at  $\theta = 0^\circ$  was always  $1.2 \times 10^5$ , at the cylinder traverse plane. See table 2 for further information about each test case.  $Dr = 1.25$ .

A further full factorial  $\Delta T_c$  nine test study was completed (coined Bc), where in contrast to the previous campaign,  $Ra_{L_c}$  at BDC was now held constant at  $1.5 \times 10^5$ . The details are given in table 3. The inner wall convective heat flux results are shown in figure 9. Conversely to figure 8, the heat flux at BDC is now relatively unchanged – the standard deviation of  $\dot{q}$  was again  $< 8 \text{ W/m}^2$ . These results corroborate the previous campaign findings that the local radial temperature difference dominates the inner wall heat transfer. This conclusion has now been confirmed at

**TABLE 3.** Thermal boundary conditions for the Bc test cases shown in figure 9. All  $\Delta T$  numbers are in Kelvin.  $Ra_{L_c}$  at  $\theta = 180^\circ$  is held constant at  $1.2 \times 10^5$  in all nine cases.

	Key	$\Delta T_{c,i}$	$\Delta T_{c,o}$	$\Delta T_{r,t}$	$\Delta T_{r,b}$	$\Delta Ra$
A	—●—	0	0	40	40	0
B	—■—	10	0	50	40	$3.7 \times 10^4$
C	—▼—	20	0	60	40	$7.2 \times 10^4$
D	—○—	0	10	30	40	$-3.7 \times 10^4$
E	—□—	10	10	40	40	0
F	—▽—	20	10	50	40	$3.4 \times 10^4$
G	—○—	0	20	20	40	$-7.1 \times 10^4$
H	—■—	10	20	30	40	$-3.4 \times 10^4$
I	—▼—	20	20	40	40	0

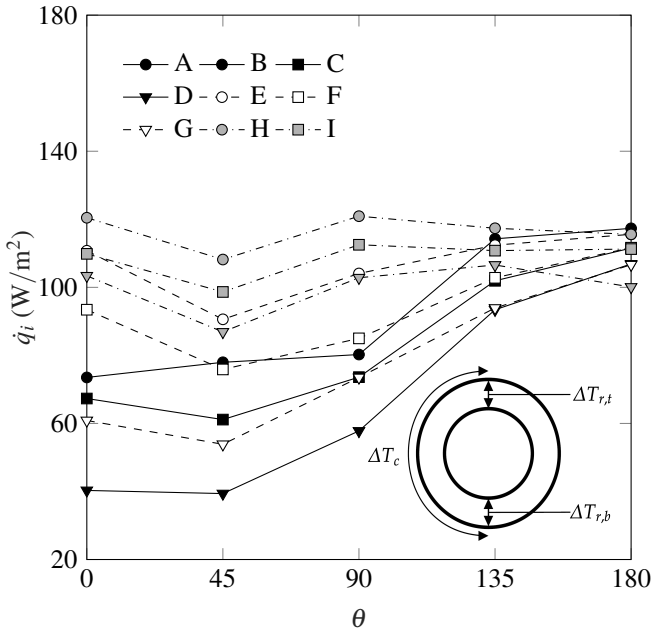


**FIGURE 9.** Inner wall convective heat flux for various thermal boundary condition tests where  $Ra_{L_c}$  at  $\theta = 180^\circ$  was always  $1.5 \times 10^5$ , at the cylinder traverse plane. See table 3 for further information about each test case.  $Dr = 1.25$ .

both TDC and BDC.

These results will now be non-dimensionalised using equation 7. Local equivalent conductivity distributions for the concentric cylinder plane at two diameter ratios are given in figure 10. The lines and filled markers represent the average of all the tests completed at that diameter ratio. Encouragingly, all of the various thermal profile case collapse down to a single trend. It was for this reason that the previous results were shown as  $\dot{q}$ , as from figure 10 it is not immediately obvious that the heat flux at

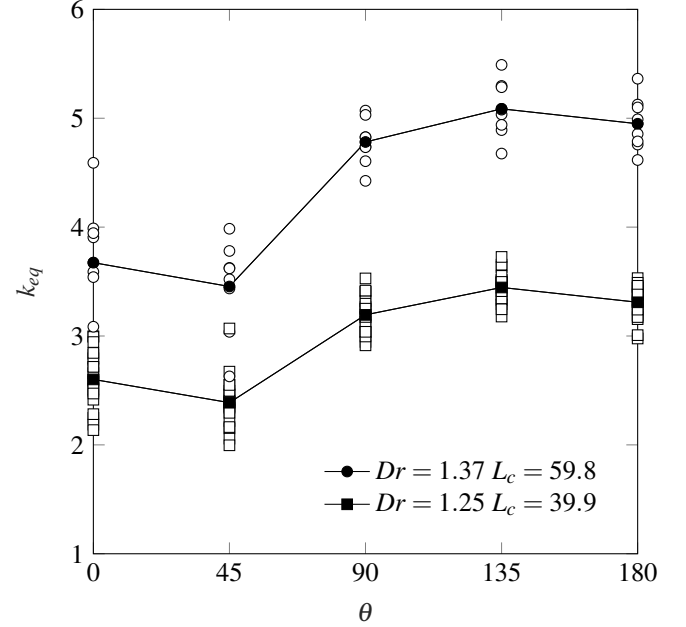


**FIGURE 10.** Inner wall equivalent conductivity for various thermal boundary condition tests in the range  $-3.5 \times 10^4 < \Delta Ra < 7.2 \times 10^4$ , at concentric cylinder plane. The filled markers are the mean of all tests at a given value of  $\theta$ . The unit of  $L_c$  is mm.

TDC may be higher than BDC (see case C in figure 8).

The distribution is very similar for both diameter ratios. The equivalent conductivity of the lower section is always higher than the upper sections – this intuitively makes sense, as this is why rotor bow occurs. The value of  $k_{eq}$  does not drop off at angles lower than  $45^\circ$ . This indicates that the flow regime is likely to be multicellular, as defined by Powe *et al.* [4].

The general profiles are again independent of the thermal boundary condition gradient. This confirms that the local radial temperature difference is the dominant variable that is driving the local heat transfer for all values of  $\theta$ , as this is having much more effect than either surface circumferential gradient,  $\Delta T_{c,i}$  or  $\Delta T_{c,o}$ , over the range of  $Ra_{L_c}$  that was tested.

### Conical Section

A similar study was completed on the conical traverse planes (see figure 2). The full Tc campaign was completed at  $Dr = 1.30$  and  $1.36$ , giving very similar trends to the concentric cylinder traverses. A subset of the Tc campaign results at  $Dr = 1.50$  are shown in figure 11.  $Ra_{L_c}$  at  $\theta = 0^\circ$  is constant here and again the standard deviation of  $\dot{q}$  at TDC was  $< 8 \text{ W/m}^2$ . However, it is interesting that there is a strong reduction in  $\dot{q}$  moving from  $45^\circ$  to TDC. This was not observed in any of the cylindrical test cases.

Figure 12 shows the inner wall equivalent conductivity for conical traverse plane test cases. The  $Dr = 1.36$  profile resembles the cylindrical cases from figure 10. The diameter ratio of this case is less than 1% smaller than the circular markers in figure 10, but the characteristic length is approx. 10% lower and thus, the values of  $k_{eq}$  are also reduced.

The sharp drop from  $45^\circ$  to TDC in the  $Dr = 1.50$  case

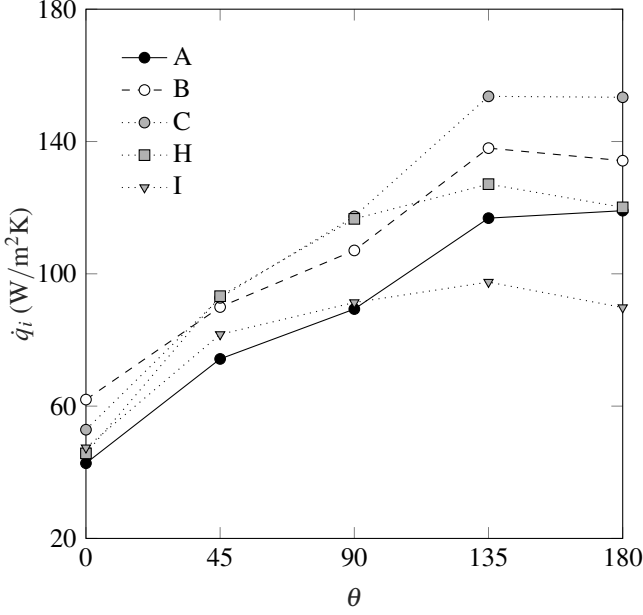


**FIGURE 11.** Inner wall convective heat flux for various thermal boundary condition tests where  $Ra_{L_c}$  at  $\theta = 0^\circ$  was always  $1.2 \times 10^5$ , at the central conical plane. See table 2 for further information about each test case.  $Dr = 1.50$ .

in again present here. This indicates that the flow regime has transitioned. This regime now likely consists of a strong central plume at  $\theta = 0^\circ$ . The temperature profiles for these tests confirm this finding. The transition value of  $Dr$  between two regimes was given as 1.24 by Angeli [3]. In this test campaign, it occurs between 1.37 and 1.50. In it unknown if the cone angle has an impact on the transition point. This transition is important as the difference in  $k_{eq}$  between TDC and BDC is much greater than the multi-cellular regime, and it is this difference in heat flux that leads to rotor bow.

While there is a slightly larger spread in this data, it is evident again that the circumferential profiles of heat flux are independent of the wall thermal boundary condition non-uniformities, even though the flow regime has transitioned.

### Overall Heat Transfer

The area-averaged equivalent conductivity values for over eighty test conditions are shown in figure 13. A correlation for natural convection between isothermal concentric cylinders from Itoh *et al.* is also included [12]. There is excellent agreement with the experimental results.

A number of important conclusions can be made based of this figure. Firstly, using  $L_c$  as defined in equation 10 as the characteristic length for the Rayleigh number is appropriate for both the concentric cylinder and conical sections, as in captured the combined effect of changing the inner diameter and the gap width. Furthermore, the conical inner section ( $5^\circ$  hade angle) does not affect the overall heat transfer. This agrees with the hypothesis of Oosthuizen [5]. Moreover, the mean surface heat transfer for non-isothermal inner and outer profiles within the range  $-0.4 < \Delta Ra/Ra_{L_c} < 0.4$ , where the thermal gradient is

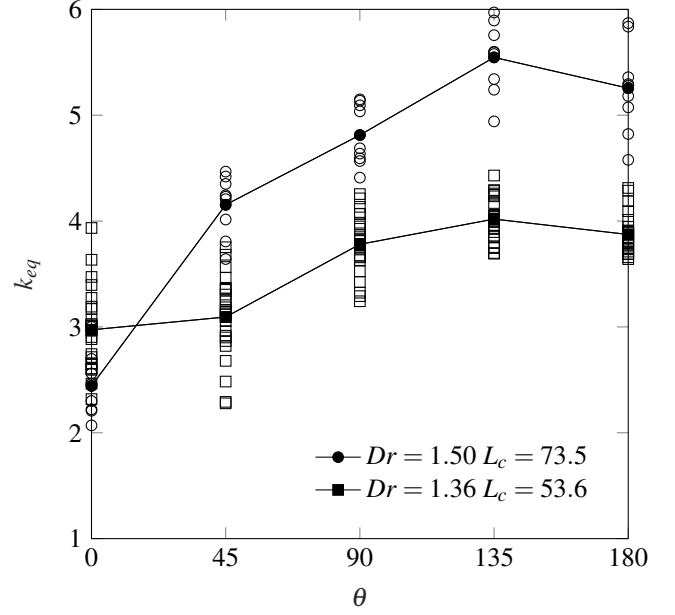


**FIGURE 12.** Inner wall equivalent conductivity for various thermal boundary condition tests in the range  $-3.5 \times 10^4 < \Delta Ra < 7.2 \times 10^4$ , at the central conical plane. The filled markers are the mean of all tests at a given value of  $\theta$ . The unit of  $L_c$  is mm.

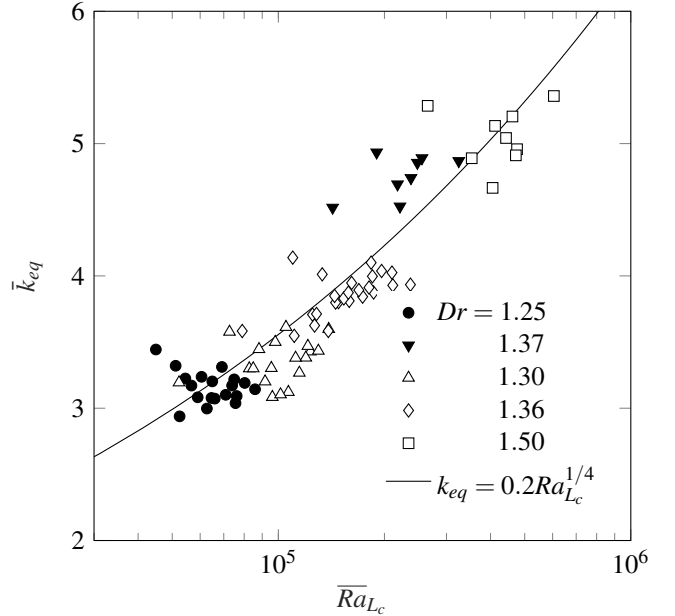


**FIGURE 13.** Mean equivalent conductivity for all thermal boundary condition tests. Filled markers were completed at the cylindrical traverse plane. White markers were completed at the conical plane. Solid line is a correlation for concentric isothermal cylinders from Itoh *et al.* [12].

negative in the  $\theta$  direction, can be predicted using isothermal correlations for  $6.5 \times 10^4 < Ra_{L_c} < 5.0 \times 10^5$ .

This trend also confirms that it is indeed the radial temperature difference dominates the local heat flux. Consequently, these findings should be applicable at lower diameter ratios than those tested, as the flow will approach a pure conduction case ( $k_{eq}=1$ ).



It is unknown at what upper limit these findings will no longer apply; therefore it should not be applied at values of  $Dr$  larger than those presented here.

## CONCLUSION

A novel experimental facility has been designed and commissioned that simulates the natural convection heat transfer that occurs in a large civil gas turbine during shutdown. The thermal boundary conditions of both walls is accurately controlled. In addition to this, a low-cost, robust thermocouple probe has been developed and validated, which allows for accurate temperature measurements in a natural convective boundary layer.

An extensive experimental campaign has been completed and numerous important findings have been observed. The key observation is that the local radial wall temperature difference was found to be the most influential parameter on the local heat transfer, at all values of  $\theta$ . Non-isothermal walls did not alter the overall distribution of the inner wall equivalent conductivity. This was true for both the cylindrical and conical sections. Furthermore, the conical inner section ( $5^\circ$  hade angle) did not affect the overall heat transfer in the range of conditions tested.

$L_c$  (as defined in equation 10) has been shown to be an appropriate characteristic length to use in the Rayleigh number definition for both the concentric cylinder and conical sections, as the mean equivalent conductivity results in figure 13 matches previously published correlations. This definition of characteristic length is matched to engine conditions, as the diameter ratio has been matched. A drawback of this version of  $L_c$  is that it does not approach  $D_i$  as  $D_o$  approaches infinity - it is known that  $D_i$  is the correct characteristic length for a horizontal cylinder in isolation. Hence,  $L_c$  should not be applied at  $Dr$ 's larger than those studied here. The correlation of Itoh is shown to be valid as far as  $Ra_{L_c} = 10^7$  [12].

Therefore, the mean surface heat transfer for non-isothermal inner and outer profiles, within the range  $-0.4 < \Delta Ra/Ra_{L_c} < 0.4$ , where the thermal gradient is negative in the  $\theta$  direction, can be predicted using isothermal correlations for  $Ra_{L_c} < 5.0 \times 10^5$  and  $Dr \leq 1.5$ .

## ACKNOWLEDGMENT

The authors would like to thank Rolls-Royce plc and the EPSRC CDT in Gas Turbine Aerodynamics for their on-going support of this project. The authors would also like to express their gratitude to the staff and technicians at the Oxford Thermofluids Institute.

## REFERENCES

- [1] E. Smith, J.H.S. de Barr, and A. Neely. 'A Sobel Sequence Parametric analysis of Rotor Thermal Bow in Gas Turbine' *Proceedings of ASME Turbo Expo 2018: Turbomachinery Technical Conference and Exposition*. Oslo, June 11-15, 2018.
- [2] A. Pilkington, B. Rosic, K. Tanimoto, and S. Horie. 'Prediction of Natural Convection Heat Transfer in Gas Tur-

- bine' *International Journal of Heat and Mass Transfer*, vol. 141, pp. 233-244, Oct 2019.
- [3] D. Angeli, G. Barozzi, M. Collins, and O. Kamiyo. 'A Critical Review of Buoyancy-induced Flow Transitions in Horizontal Annuli' *International Journal of Thermal Sciences*, vol. 49, no. 12, pp. 2231-2241, Dec 2010.
- [4] R. E. Powe, C. T. Carley, and E. H. Bishop. 'Free Convective Flow Patterns in Cylindrical Annuli' *Journal of Heat Transfer*, vol. 91, no. 3, pp. 310-314, Aug 1969.
- [5] P. H. Oosthuizen, 'Free Convective Heat Transfer From Horizontal Cones' *Journal of Heat Transfer*, vol. 95, no. 3, pp. 409-410, Aug 1973.
- [6] D. D. Fahy, P. T. Ireland, L. V. Lewis, and E. Raya. 'A Novel Experimental Technique for Investigating Natural Convective Heat Transfer in a Gas Turbine Annulus' *Proceedings of ASME Turbo Expo 2018: Turbomachinery Technical Conference and Exposition*. Oslo, June 11-15, 2018.
- [7] W. George and S. Capp. 'A Theory for Natural Convection Turbulent Boundary Layers next to Heated Vertical Surfaces' *International Journal of Heat and Mass Transfer* vol. 22, pp. 813-826, 1979.
- [8] K. S. Kulkarni, U. Madanan, T. W. Simon, and R. J. Goldstein. 'Experimental Validation of a Boundary Layer Convective Heat Flux Measurement Technique' *Journal of Heat Transfer*, vol. 140, no. 7, p. 074501, July 2018.
- [9] K. S. Kulkarni, S. Han, and R. J. Goldstein. 'Numerical Simulation of Thermal Boundary Layer Profile Measurement' *International Journal of Heat and Mass Transfer*, vol. 47, no. 8, pp. 869-877, Aug 2011
- [10] J. R. Taylor. 'An Introduction to Error Analysis: The Study of Uncertainties in Physical Measurements' 2nd edition. *University Science Books*, 1996.
- [11] T. H. Kuehn and R. J. Goldstein. 'An Experimental and Theoretical Study of Natural Convection in the Annulus between Horizontal Concentric Cylinders' *Journal of Fluid Mechanics* vol. 74, no. 4, pp. 695-719, Apr 1976.
- [12] M. Itoh, N. Nishiwaki, and M. Hirata. 'A new Method of Correlating Heat Transfer Coefficients for Natural Convection in Horizontal Cylindrical Annuli' *International Journal of Heat and Mass Transfer*, vol. 13, pp. 1364-1368, Aug 1970.